

Realistic numerical simulations of solar convection and oscillations in magnetic regions

L. Jacoutot¹, A. G. Kosovichev², A. Wray³, & N. N. Mansour³

¹Center for Turbulence Research, Stanford University, Stanford, CA 94305

²Hansen Experimental Physics Laboratory, Stanford University, Stanford, CA 94305

³NASA Ames Research Center, Moffett Field, CA 94035

ABSTRACT

The goal of this research is to investigate how magnetic field affects the dynamics of granular convection and excitation of solar oscillations by means of realistic numerical simulations. We have used a 3D, compressible, non-linear radiative magnetohydrodynamics code developed at the NASA Ames Research Center. This code takes into account several physical phenomena: compressible fluid flow in a highly stratified medium, sub-grid scale turbulence models, radiative energy transfer between the fluid elements, and a real-gas equation of state. We have studied the influence of the magnetic field of various strength on the convective cells and on the excitation mechanisms of the acoustic oscillations by calculating spectral properties of the convective motions and oscillations. The results reveal substantial changes of the granulation structure with increased magnetic field, and a frequency-dependent reduction in the oscillation power in a good agreement with solar observations. These simulations suggest that the enhanced high-frequency acoustic emission at the boundaries of active region ("acoustic halo" phenomenon) is caused by the changes of the spatial-temporal spectrum of the turbulent convection in magnetic field, resulting in turbulent motions of smaller scales and higher frequencies than in quiet Sun regions.

Subject headings: convection | methods: numerical | Sun: oscillations

1. Introduction

Observations of solar oscillations have revealed that their properties change significantly in magnetic regions (Brown et al. 1992). Using SOHO /MDI data Hindman & Brown (1998) found that the power of Doppler-velocity oscillations with frequencies less than 5.2 mHz (which corresponds to the acoustic cut-off frequency) decreases with field strength, but the

oscillations at higher frequencies become stronger. The regions of enhanced high-frequency oscillation power are usually observed at the boundaries of active regions and are sometimes referred as "halos". Similar effect was found for local oscillation modes by Howe et al. (2004), who also found that in magnetic regions the line width of acoustic modes increases at low frequencies and decreases at high frequencies. The interpretation of these results is not clear. These variations can be caused by the interaction of acoustic waves with magnetic field and also by changes in the properties of solar convection and excitation mechanism of acoustic waves. It is well-known that magnetic field inhibits convection, thus causing the reduction in the power of acoustic waves produced by the turbulent convective motions. However, the details of this process are unknown. We address this problem by using realistic numerical simulations of solar convection in the presence of magnetic field. The realistic numerical simulations pioneered by Stein & Nordlund (2001) have provided an important insight into the excitation mechanism of oscillations on the Sun and solar-type stars, showing that the acoustic modes by the work of turbulent pressure (Reynolds stresses) and nonadiabatic gas pressure (entropy) fluctuations (Stein et al. 2004). Of course, the numerical simulation must rely on sub-grid scale models of turbulence. Jacoutot et al. (2008) investigated various turbulence models and showed that the dynamic model of Moïn et al. (1991) provides the best agreement with solar observations. In this paper, we include magnetic field in the realistic simulations and investigate changes in the physical properties of convection and oscillations.

2. Numerical model

We use a 3-D, compressible, non-linear radiative-magnetohydrodynamics code developed by Dr. A. Wray for simulating the upper solar convection zone and lower atmosphere. This code takes into account several physical phenomena: compressible fluid flow in a highly stratified medium, radiative energy transfer between the fluid elements, a real-gas equation of state, and magnetic effects. Direct numerical simulation (DNS) of the high Reynolds-number turbulent motions on the Sun is not achievable. It is not possible to resolve all the motion scales even with the most advanced computers. The large-eddy simulation (LES) method allows overcoming the Reynolds-number limits possible for DNS by modeling the effects of the smallest turbulent scales. Thus, LES method is used in the present calculations.

The equations we solve are the grid-cell averaged (henceforth called "averages") conservations of mass (1), momentum (2), energy (3), and magnetic flux (4):

$$\frac{\partial}{\partial t} + (\mathbf{u}_i)_{;i} = 0; \quad (1)$$

$$\frac{\partial u_i}{\partial t} + (u_i u_j + (P_{ij} + \tau_{ij}))_{,j} = \rho_i \dot{r}_i \quad (2)$$

$$\frac{\partial E}{\partial t} + E u_i + (P_{ij} + \tau_{ij}) u_j - (\kappa + \kappa_T) T_{,i} + \frac{c^2}{4} \frac{1}{\kappa + \kappa_T} (B_{ij} - B_{ji}) B_{,j} + F_i^{\text{rad}} = 0; \quad (3)$$

$$\frac{\partial B_i}{\partial t} + u_j B_{,i} - u_i B_{,j} - \frac{c^2}{4(\kappa + \kappa_T)} (B_{ij} - B_{ji})_{,j} = 0; \quad (4)$$

where ρ is the averaged mass density, u_i is the Favre-averaged velocity, B_i is the magnetic field, and E is the averaged total energy density $E = \frac{1}{2} u_i u_i + e + \frac{1}{8} B_i B_i$, where Φ is the gravitational potential and e is the Favre-averaged internal energy density per unit mass. F_i^{rad} is the radiative flux, which is calculated by solving the radiative transfer equation, and P_{ij} is the averaged stress tensor $P_{ij} = p + 2 u_{k,k} \tau_{ij} + \frac{1}{8} B_k B_{k,ij} - \frac{1}{4} B_i B_{,j}$, where τ is the viscosity. The gas pressure p is a function of e and Φ through a tabulated equation of state (Rogers et al. 1996); τ_{ij} is the Reynolds stress, κ is the molecular thermal conductivity, κ_T is the turbulent thermal conductivity, σ is the molecular electrical conductivity, and σ_T is the turbulent electrical conductivity.

We have carried out simulations using the most widely used subgrid-scale models (SGS): the Smagorinsky model (Smagorinsky 1963). The Reynolds stresses τ_{ij} are modeled by the usual eddy viscosity assumption using the large-scale stress tensor $S_{ij} = (u_{i,j} + u_{j,i})/2$:

$$\tau_{ij} = \frac{1}{3} \kappa_{kk} \delta_{ij} = -2\tau S_{ij} - \frac{1}{3} S_{kk} \delta_{ij} \quad (5)$$

The eddy viscosity τ is defined by the Smagorinsky model (Smagorinsky 1963), $\tau = C_S \Delta^2 \mathcal{P}$ and the trace of the subgrid Reynolds stress κ_{kk} is modeled using the Yoshizawa's expression (Yoshizawa 1986): $\kappa_{kk} = 2C_S \Delta^2 \mathcal{P}^2$, where $\mathcal{P} = \sqrt{2S_{ij}S_{ij}}$ and $(x, y, z)^{1=3}$, x , y , and z are the grid step sizes.

The application of the eddy viscosity, τ , and the subgrid kinetic energy, κ_{kk} , results in the compressible Smagorinsky formulation (Moin et al. 1991):

$$\tau_{ij} = -2C_S \Delta^2 \mathcal{P} (S_{ij} - u_{k,k} \delta_{ij}/3) + 2C_C \Delta^2 \mathcal{P}^2 \delta_{ij}/3; \quad (6)$$

where C_S is the classical Smagorinsky coefficient as used in incompressible flow modeling; and C_C is a coefficient associated with the trace of the subgrid Reynolds stress (which is absent in the incompressible flow formulation). The two parameters must be specified in some way. For the original Smagorinsky model, constant values are used. In the present work, we have chosen $C_S = 0.2$ and $C_C = 0.1$.

The turbulent Prandtl number was taken as unity to set κ_T . The molecular viscosity and thermal conductivity were neglected as their solar values are exceedingly small.

The turbulent electrical conductivity η_T is calculated by using the extension of the Smagorinsky model to the MHD case (Theobald et al. 1994), with the flow velocity shear replaced by a shear of the magnetic field (which is the electric current): $\eta_T = C_B^{-2} \sum_{ijk} j_i^2$ with $j_i = \epsilon_{ijk} B_{k,j}$ is the resolved electric current; ϵ_{ijk} is the Levi-Civita symbol; C_B was taken equal to 1. (Theobald et al. 1994).

In all the following sections, we simulate the upper layers of the convection zone using $66 \times 66 \times 66$ grid cells. The region extends 6×6 Mm horizontally and from 5.5 Mm below the visible surface to 0.5 Mm above the surface. The initial magnetic field is imposed as a vertical uniform component on a snapshot of the preexisting hydrodynamic convection, calculated as described in Jacoutot et al. (2008). The initial values of the field strength are: 100, 300, 600, and 1200 Gauss. The weak field of 100 G has almost no effect. Thus, we present here the three other cases.

3. Granulation structure

The first step was to investigate the influence of the initial magnetic field on the granular structure of convection. Figure 1 shows temperature, vertical velocity, and vertical magnetic field distributions at the visible surface for different magnetic fields. We observe that the size of granules decreases as the initial magnetic field increases. Without magnetic field the mean size of granules is about 2 Mm, and it is less than 0.75 Mm for 1200 Gauss. In addition, the temperature in the granules becomes higher as the initial magnetic field increases. We can also note that the down-flow in the intergranular lanes is weaker for high magnetic fields. Figure 2, which shows the vertical velocity energy as a function of the horizontal wavelength, k_h , measured in degrees of spherical harmonics, $l = k_h R_\odot$, demonstrates this feature. The vertical velocity energy is decreased by a factor of 10^3 for small values l , which correspond to the larger granules. We can also notice that the magnetic field is swept into the intergranular lanes although the magnetic field is seeded uniformly. This characteristic of solar magnetoconvection is well-known and has already been presented by Stein & Nordlund (2002).

4. Kinetic energy and oscillation power of radial modes

We then studied how the kinetic energy is dissipated for different initial magnetic field. To do this, we calculated the oscillation power spectra of radial modes. Those modes are extracted by horizontally averaging the vertical velocity and Fourier-transforming in time.

These results are obtained from simulations of 60 hours of solar time using instantaneous snapshots saved every 30 seconds. Five oscillation modes can be clearly seen as sharp peaks in the spectra of the horizontally averaged, depth-integrated kinetic energy (Fig. 3) and the power spectrum of the vertical velocity oscillations at the solar surface (Fig. 4). The smallest resonant mode frequency is 2.07 mHz. This mode is excited along all the depth. The resonant frequencies supported by the computational box are 2.07, 3.03, 4.10, 5.23, 6.52 mHz. In addition, several broad high-frequency peaks at 6–12 mHz corresponding to pseudo-modes (Kumar & Lu 1991) can be identified.

It is clear that the magnetic field significantly affects the kinetic energy spectrum. The amplitude of the excited modes decreases as the initial magnetic field increases, as well as the total oscillation power (Fig. 5). The power distribution is shifted towards higher frequencies with the increase of the field strength. It is particularly interesting that the amplitude of the pseudo-modes increases with field strength and reaches maximum at $B_{z0} = 600$ G. This may explain the effect of enhanced high-frequency emission ("acoustic halos") around active regions (Brown et al. 1992; Hindman & Brown 1998; Jain & Haber 2002). The enhanced emission at frequencies 5–7 mHz appears at the boundaries of active regions where magnetic field is moderate. This corresponds to the simulations results: the pseudo-mode amplitude is high for 600 G field and diminishes at 1200 G.

The simulations also show the enhanced spectral power of the convective background at high frequencies for models with magnetic field, forming plateaux at > 6 mHz. This leads to the idea that the acoustic halos are caused by enhanced high-frequency turbulent convective motions in the presence of moderate magnetic field. This is consistent with the decreased granular size in magnetic regions, described in the previous section. The smaller scale convection naturally has higher frequencies and, thus, generates more higher frequency acoustic waves than convection without magnetic field. When the field is very strong the sound generation decreases because of suppression of convective motions of all scales. This probably explains why the acoustic halos are observed in regions of moderate magnetic field strength at the boundaries of active regions.

In addition, the simulation results show that the modal lines in the oscillation power spectrum (Fig. 4) become broader for the mode of 2.07 and 3.03 mHz (the first mode almost disappears at $B_{z0} = 1200$ G), but they are more narrow for the modes of 4.10, 5.23, 6.52 mHz. This qualitatively corresponds to the observational result of Howe et al. (2004). We plan to present a quantitative analysis in a future publication.

5. Calculation of the p-m ode work integrand

The dominant driving of the p-m odes comes from the interaction of the non-adiabatic, incoherent pressure uctuations with the coherent mode displacement (Nordlund & Stein 2001). Previous work of Balmer (1992), Goldreich et al. (1994), Kumar (1994), Nordlund & Stein (1998) showed that turbulent motions stochastically excite the resonant modes via Reynolds stresses (turbulent pressure) and entropy uctuations (gas pressure). Many analytical formulations have been proposed by Balmer (1992); Goldreich et al. (1994); Samadi & Goupil (2001). The problem is that these models introduce free parameters related to the choice of the turbulent medium model. The advantage of 3-D realistic numerical simulations comes from the possibility of calculating all the quantities related to turbulent convection. Nordlund & Stein (2001) presented a formalism for analyzing the interaction of convection with purely radial oscillations. This formalism seems to be the most accurate because it accounts for phase relations between pressure uctuations (both turbulent and gas) and the mode compression factor $\partial \xi / \partial r$ (Stein et al. 2004). In this section the mode excitation rate is calculated using the same method, but we add the contribution of the magnetic pressure $\frac{1}{8} B_k B_k$ in the calculation of the total pressure. The rate of energy input to the modes per unit surface area ($\text{erg cm}^{-2} \text{s}^{-1}$) is

$$\frac{\langle E_l \rangle}{t} = \frac{\int_0^R \frac{1}{8} \frac{P_l^2}{E_l} dr}{E_l}; \quad (7)$$

where P_l is the Fourier transform of the non-adiabatic total pressure; \int in front of the pressure means that one computes so-called ‘pseudo-Lagrangian’ uctuations relative to a fixed mass radial coordinate system (Nordlund & Stein 2001); $\Delta \omega$ is the frequency interval for the Fourier transform; ξ_l is the mode displacement for the radial mode of angular frequency ω . It is obtained from the eigenmode calculations for a standard solar model of Christensen-Dalsgaard et al. (1996). His spherically symmetric model S gives 35 radial modes that provide much denser frequency spectrum in comparison with the three resonant modes obtained within the simulation box. E_l is the mode energy per unit surface area (erg cm^{-2}) defined as:

$$E_l = \frac{1}{2} \int_0^R \rho \left(\frac{d\xi_l}{dr} \right)^2 dr + \frac{1}{2} \frac{\xi_l^2}{R}; \quad (8)$$

The distributions of the integrand of the work integral as a function of depth and frequency (Figure 6) are similar to the results obtained by Stein & Nordlund (2001). Most driving is concentrated between the surface and 500 km depth at around 3-4 mHz. We can see that the excitation becomes weaker for high initial magnetic field. The contribution of the different pressures (gas, turbulent and magnetic) is presented in Fig.7. We see that the dominant driving comes from the interaction of the coherent mode displacement with

the non-adiabatic, incoherent gas pressure fluctuations. The contribution of the turbulent pressure shows similar shape than that of the gas pressure, but it is weaker. The magnetic pressure plays a weak role in the excitation of the p-modes for 300 Gauss. This contribution becomes higher with increased magnetic field. The total work integrand with increased magnetic field becomes localized closer to the surface and at the mode frequencies.

6. Conclusion

We have carried out realistic simulations of solar convection and oscillation in the presence of magnetic field of various strength. Initially, the magnetic field was vertical and uniformly distributed. The results reproduced several phenomena observed in solar magnetic regions.

In particular, the results confirm that the spatial scale of granulation substantially decreases with the magnetic field strength. Magnetic field is swept in the intergranular lanes, and the vertical downdraft motions in these lanes are suppressed. This results in a decrease in the excitation power. The oscillation power in the presence of magnetic field is shifted towards higher frequencies, also increasing the amplitude of pseudo-modes above the acoustic cut-off frequency. At a moderate field strength of 600 G the power of the high-frequency oscillations reaches a maximum. This corresponds to the phenomenon of "acoustic halo" observed in the range of 5–7 mHz at the boundaries of active regions. The reason of this phenomenon is probably in the change of the spatial-temporal spectrum of the turbulent convection in magnetic field. The convective motions become smaller in spatial scale and faster in the presence of magnetic field, and this causes the changes in the oscillations excited by these motions.

The power spectra show a significant increase of the convective power ("plateau") at high frequencies. The oscillation modal lines become broader and smaller in amplitude for the low-frequencies modes, but more narrow at higher frequencies. Qualitatively, this corresponds to the observations, but requires a more detailed quantitative study.

The calculations of the work integrand show that the excitation mechanism in magnetic regions remains the same as in the quiet Sun. The oscillations are excited by fluctuations of Reynolds stresses and entropy with magnetic forces playing a minor role. With increased magnetic field the work integrand becomes more concentrated in the near-surface layers and at the mode frequencies.

In general, our simulations lead to a conclusion that the observed changes of solar oscillations in magnetic regions on the Sun are mostly caused by changes in the spatial-

temporal spectrum of convective motions, which are the source of the oscillations.

REFERENCES

- Brown, T.M., Bogdan, T.J., Lites, B.W., & Thomas, J.H. 1992, *ApJ*, 394, L65
- Hindman, B.W., & Brown, T.M. 1998, *ApJ*, 504, 1029
- Balmforth, N.J., 1992, *MNRAS*, 255, 639
- Christensen-Dalsgaard, J., et al. 1996, *Science*, 272, 1286
- Goldreich, P., Murray, N., & Kumar, P. 1994, *ApJ*, 424, 466
- Howe, R., Komm, R.W., Hill, F., Haber, D.A., & Hindman, B.W. 2004, *ApJ*, 608, 562
- Jacoutot, L., Kosovichev, A.G., Wray, A., & Mansour, N.N. 2008, *ApJ*, in press; *ArXiv e-prints*, 710, [arXiv:0710.2317](https://arxiv.org/abs/0710.2317)
- Jain, R., & Haber, D. 2002, *A & A*, 387, 1092
- Kumar, P., & Lu, E. 1991, *ApJ*, 375, L35
- Kumar, P. 1994, *ApJ*, 428, 827
- Moin, P., Squires, K., Cabot, W., & Lee, S. 1991, *Phys. Fluids A*, 3, 11, 2746
- Nordlund, A., & Stein, R.F. 1998, in *IAU Symp. 185: new eyes to see inside the sun and stars*, 199
- Nordlund, A., & Stein, R.F. 2001, *ApJ*, 546, 576
- Rogers, F.J., Swenson, F.J. & Iglesias, C.A. 1996, *ApJ*, 456, 902
- Samadi, R., & Goupil, M.-J. 2001, *A & A*, 370, 136
- Smagorinsky, J., 1963, General circulation experiments with the primitive equations, *Monthly Weather Review*, 93, 99
- Stein, R.F. & Nordlund, A. 2001, *ApJ*, 546, 585
- Stein, R.F. & Nordlund, A. 2002, *SOLMAG. Proceedings of the Magnetic Coupling of the Solar Atmosphere Euroconference*, 505, 83-89

Stein, R . F . , Georgobiani, D . , Trampedach, R . , Ludwig, H .-G . & Nordlund, A . 2004, Solar Physics, 220, 229

Theobald, M . L . , Fox, P . A . , Sosa, S . 1994, Phys. Plasmas, 1, 9

Yoshizawa, A . 1986, Phys. Fluids, 29, 2152

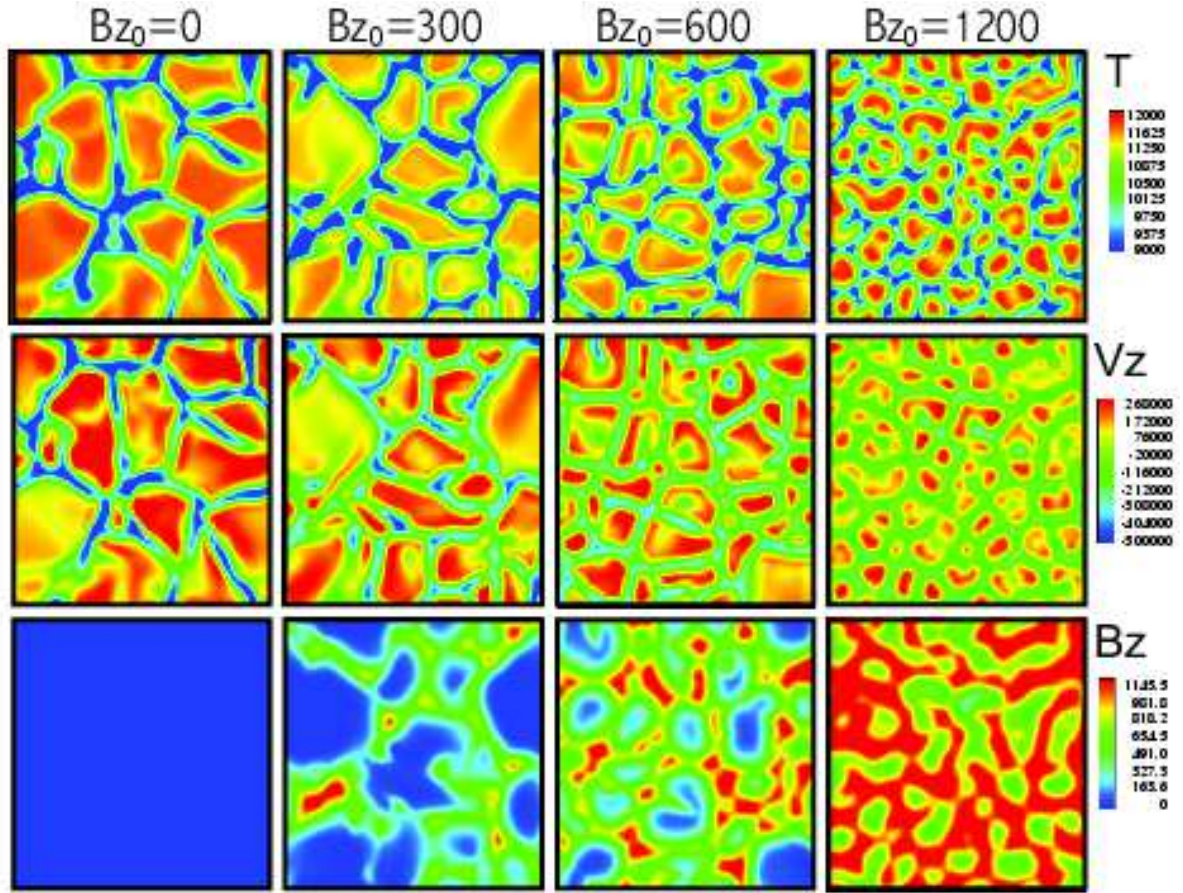


Fig. 1. | Temperature (K), vertical velocity (cm/s) and vertical magnetic field (Gauss) distributions at the visible surface for different initial vertical magnetic fields.

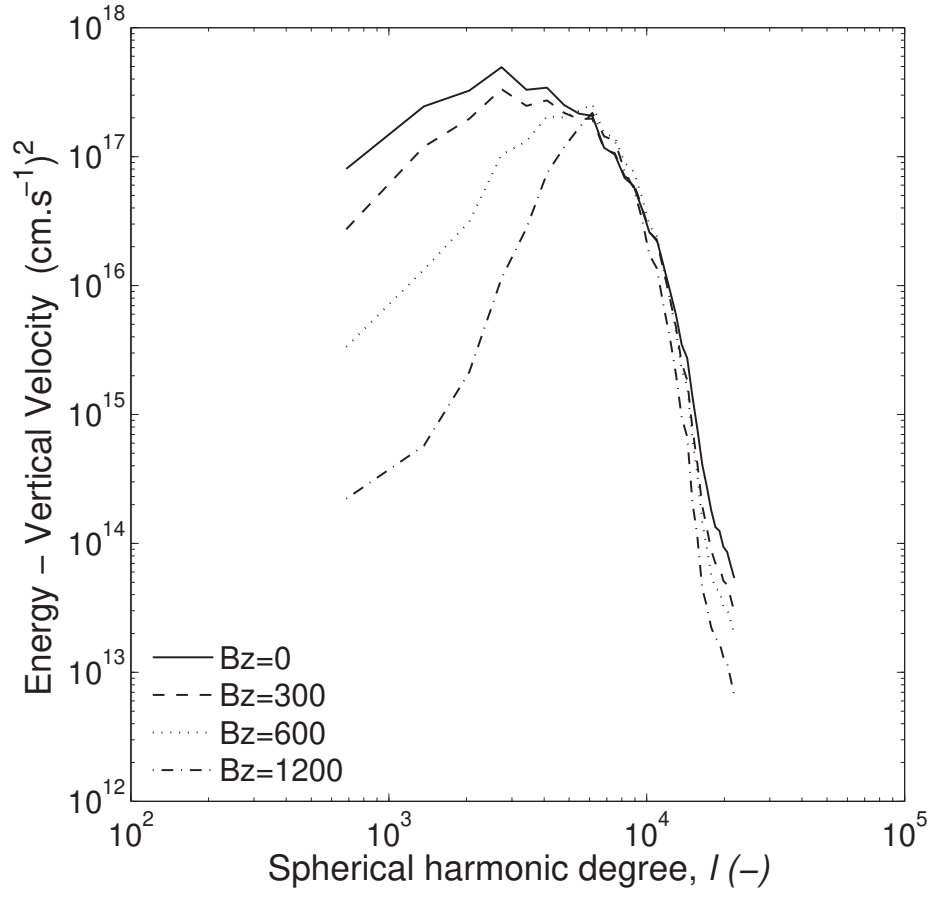


Fig. 2. | Spatial energy of the vertical velocity as a function of the spherical harmonic degree l at the visible surface for different initial vertical magnetic fields.

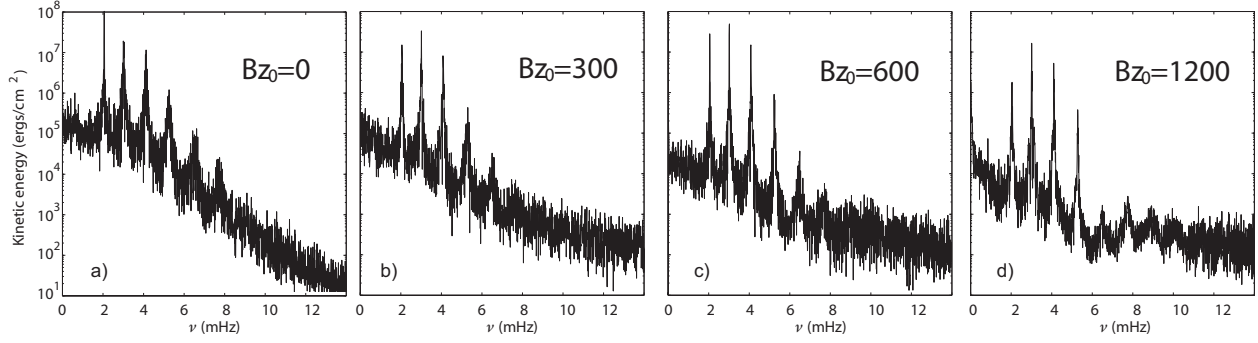


Fig. 3. | Kinetic energy spectra integrated over depth for different initial vertical magnetic fields.

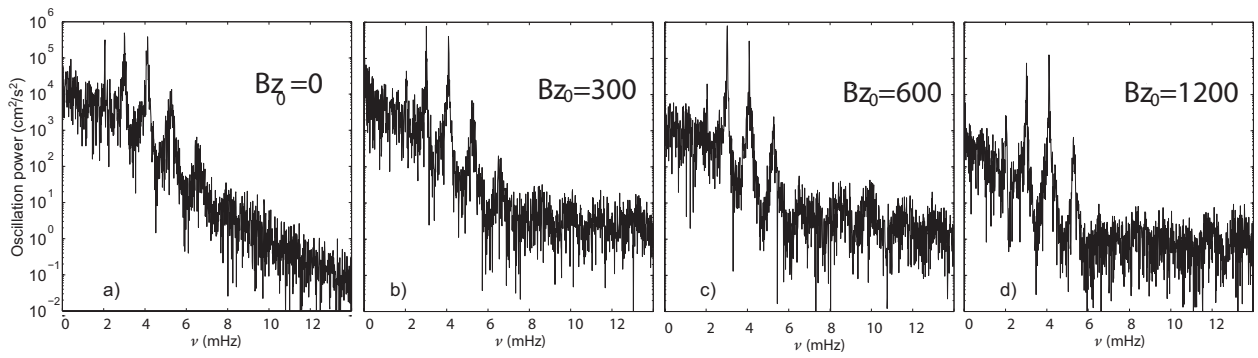


Fig. 4. | Oscillation power spectra at the visible surface for different initial vertical magnetic fields.

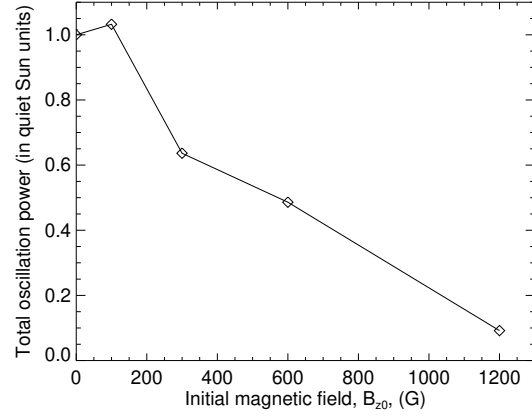


Fig. 5. Total oscillation power at the visible surface as a function of initial magnetic field strength.

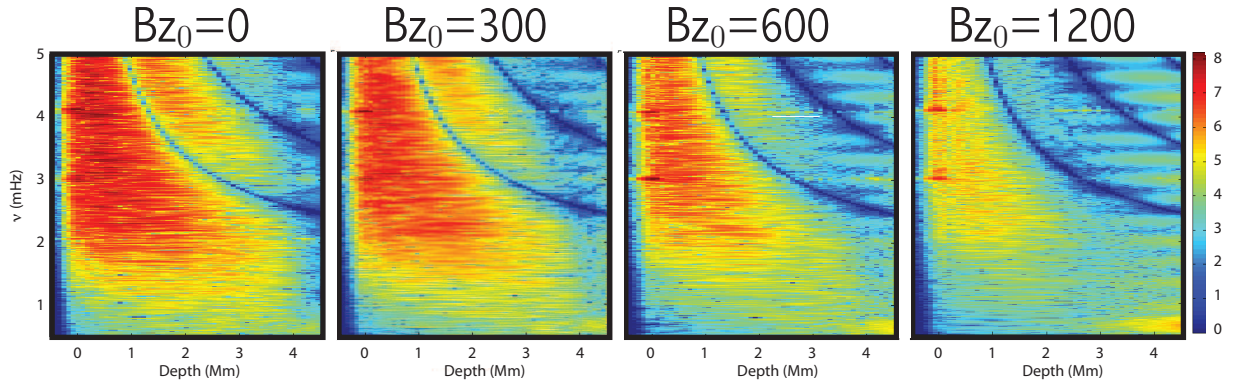


Fig. 6. Logarithm of the total work integrand (eq. (7) in units of $\text{erg cm}^{-2} \text{s}^{-1}$), as a function of depth and frequency for different initial vertical magnetic field.

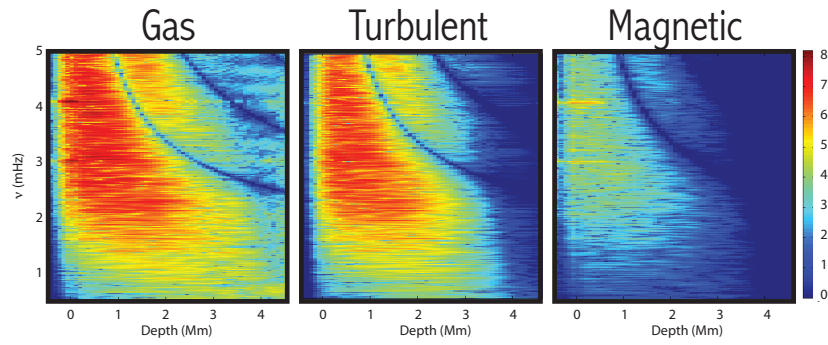


Fig. 7. | Gas, turbulent and magnetic pressure contributions in the work integrand (in units of $\text{erg cm}^{-2} \text{s}^{-1}$), as a function of depth and frequency for an initial vertical magnetic field of 300 Gauss.